TGF-β Regulates Cathepsin Activation during Normal and Pathogenic Development

Heather Flanagan-Steet[1,6,*], **Courtney Christian**[1,3], **Po-Nien Lu**[1,3], **Megan Aarnio-Peterson**[1], **Laura Sanman**[2,5], **Stephanie Archer-Hartmann**[1], **Parastoo Azadi**[1], **Matthew Bogyo**[2], and **Richard A. Steet**[1,4]

[1]Complex Carbohydrate Research Center, University of Georgia, Athens, GA 30606, USA

[2]Department of Pathology, Stanford University School of Medicine, Stanford, CA 94305-5324, USA

[3]These authors contributed equally

[4]Senior author

[5]Present address: School of Pharmacy, University of California, San Francisco, San Francisco, CA 94158, USA

[6]Lead Contact

SUMMARY

Cysteine cathepsins play roles during development and disease beyond their function in lysosomal protein turnover. Here, we leverage a fluorescent activity-based probe (ABP), BMV109, to track cysteine cathepsins in normal and diseased zebrafish embryos. Using this probe in a model of mucolipidosis II, we show that loss of carbohydrate-dependent lysosomal sorting alters the activity of several cathepsin proteases. The data support a pathogenic mechanism where TGF-β signals enhance the proteolytic processing of pro-Ctsk by modulating the expression of chondroitin 4-sulfate (C4-S). In MLII, elevated C4-S corresponds with TGF-β-mediated increases in *chst11* expression. Inhibiting *chst11* impairs the proteolytic activation of Ctsk and alleviates the MLII phenotypes. These findings uncover a regulatory loop between TGF-β signaling and Ctsk activation that is altered in the context of lysosomal disease. This work highlights the power of ABPs to identify mechanisms underlying pathogenic development in living animals.

In Brief

Chondroitin sulfate is a known regulator of cathepsin protease activity. Flanagan-Steet et al. identify a positive feedback mechanism whereby cathepsins secreted from chondrocytes upon loss of lysosomal targeting activate TGF-β signaling in developing cartilage. This increased signaling, in turn, stimulates chondroitin-4 sulfation and enhances cathepsin activity.

Graphical Abstract
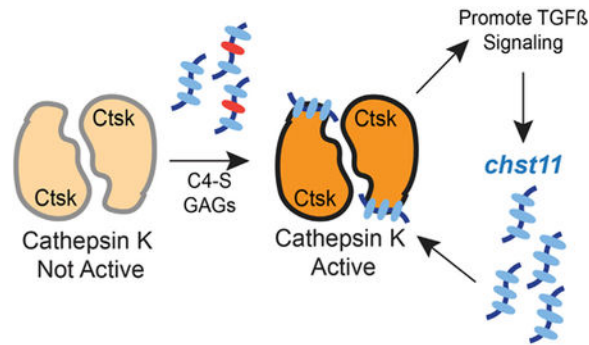
INTRODUCTION

Cysteine cathepsins play essential roles in biological processes beyond lysosomal protein turnover (Reiser et al., 2010). Studies of cellular and developmental systems identified numerous functions for these proteases, including hormone and neuropeptide processing, antigen presentation, and growth factor activation and stability (Flanagan-Steet et al., 2016; Honey and Rudensky, 2003; Hook et al., 2008). Inappropriate expression or loss of cathepsins are associated with metastatic cancer, atherosclerosis, neurodegenerative diseases, rheumatoid arthritis, chronic inflammatory lung disease, and lysosomal storage disorders (Ketterer et al., 2017; Liu et al., 2004; Lutgens et al., 2007; Olson and Joyce, 2015; Stoka et al., 2016; Vasiljeva et al., 2007; Wilson and Brömme, 2010; Zhang et al., 2011). Because cathepsins perform functions in and out of the lysosome, defining how their expression, intracellular sorting, and activation are regulated is essential to fully understand their biological function. Activity-based probes (ABPs) provide a powerful way to directly monitor protease activity in the context of living cells and organisms (Edgington-Mitchell et al., 2017; Kato et al., 2005; Sanman and Bogyo, 2014). ABPs are small-molecule reporters that covalently and irreversibly attach to the active-site nucleophile of target enzymes. When "unbound," an intrinsic quenching group inhibits the fluorescence capacity of the probe. Interaction with the target enzyme's active site displaces this group, causing the probe to fluoresce.

Mucolipidosis II (MLII) is a lysosomal storage disorder caused by mutations in the GNPTAB gene encoding the GlcNAc-1-phosphotransferase enzyme. The GlcNAc-1-phosphotransferase catalyzes the addition of a mannose 6-phosphate (M6P) tag to the N-glycans of newly synthesized hydrolases, directing their transport to lysosomes (Kollmann et al., 2010; Kornfeld and Mellman, 1989; Reitman et al., 1981; Tiede et al., 2005). Loss of this phosphotransferase enzyme impairs lysosomal targeting, causing the hydrolases to be

secreted from the cell. Intracellular hydrolase deficiency leads to tissue-specific macromolecular storage. Although profound lysosomal storage is the hallmark of MLII, recent data implicate a role for secreted cathepsins in early disease pathology (Flanagan-Steet et al., 2016; Petrey et al., 2012). Studies in zebrafish demonstrate that, when mislocalized outside cells, cathepsin K (Ctsk) becomes hyperactivated and increases transforming growth factor β (TGF-β)-related signaling (Flanagan-Steet et al., 2016). Although inhibiting Ctsk improves MLII cartilage, it is unclear whether additional secreted cathepsins contribute to the MLII phenotypes. Moreover, the molecular mechanisms linking cathepsin activation to TGF-β signaling are unknown.

Taking advantage of a cathepsin-specific ABP (BMV109) (Verdoes et al., 2013), we assessed the breadth of protease activities in embryonic zebrafish during normal and pathogenic development. Our findings confirm MLII-increased Ctsk and identify additional cathepsins whose activities are altered when M6P biosynthesis is reduced. We further show that TGF-β signaling reciprocally regulates Ctsk activity. Inhibiting TGF-β signaling in either wild-type (WT) or MLII embryos impaired Ctsk processing, reducing its activity. TGF-β mediates its effect on Ctsk by increasing expression of the primary sulfotransferase (*chst11*) that generates chondroitin 4-sulfate (C4-S), a known Ctsk modulator (Lemaire et al., 2014; Li et al., 2000, 2004). This work identifies a regulatory loop between cathepsins and TGF-β signaling in developing cartilage that is disrupted when lysosomal targeting is impaired. The implications of these findings regarding protease-mediated tissue development and lysosomal disease pathogenesis are discussed.

RESULTS

BMV109 Uncovers Dynamic Cathepsin Activation during Development

To investigate cathepsin dynamics during development, we temporally tracked activity in zebrafish embryos using the ABP BMV109 (Figure 1A). BMV109 contains a Cy5 moiety whose fluorescence is quenched until the probe binds activated cysteine cathepsins (Verdoes et al., 2013). BMV109's efficacy in zebrafish was demonstrated by microinjection into either the yolk or cell of 0 hours post fertilization (hpf) embryos (Figure 1B). In-gel analyses of Cy5 fluorescence from embryonic lysates revealed multiple probe-reactive bands. These bands not only spanned the predicted molecular weights of several mature cathepsins (15–30 kDa) but were also all competitively inhibited by the cysteine cathepsin inhibitor E64d. Comparison of embryos harvested 1 and 2 days post-injection (dpi) showed that the reactivity of several lower-molecular-weight proteins increases after longer incubation periods. These analyses also revealed differences in labeling efficiency between yolk- and cell-injected samples, with cell-injected samples being more efficiently labeled.

When bound, BMV109 is an irreversible inhibitor. Therefore, to maximize probe delivery in older embryos and minimize the effect on cathepsin-dependent biological processes, additional labeling strategies were evaluated. BMV109 was injected either into the yolks or bloodstream of 1-day-old (24 hpf) embryos (Figures 1C and 1D), and the extent of labeling was analyzed in gels and by live confocal microscopy. Delivering the probe into the bloodstream via pericardial injection consistently increased reactivity with several proteases (arrowheads, Figure 1C). Although only 30% of yolk-injected embryos showed labeling in

distant structures like craniofacial cartilages or the forebrain, 92% of the embryos injected pericardially had strong labeling in all embryonic tissues within 15 hr (Figure 1D). When injected pericardially, BMV109 reactivity was noted in the craniofacia and jaw (R1 and R2; Figure 1D), the brain (R3; Figure 1D), the heart (R4; Figure 1D), the myotomal segments, and the ventral tail (R5; Figure 1C). BMV109 delivery was analyzed with *fli1a*:EGFP in transgenic zebrafish, which labels multiple tissues with EGFP. Gross alterations in tissue morphology were never detected, suggesting that, at this concentration, BMV109 efficiently reports protease activity without completely inhibiting it. For subsequent analyses, BMV109 was introduced into the cell (for 0- to 1-day embryos) or pericardium (for 1- to 5-day embryos).

Cts Activities Fluctuate during Development

ABPs covalently label their target, allowing tagged proteases to be identified. Using a combination of immunoprecipitation, morpholino knockdown, and cathepsin-specific ABPs, we determined the identities of several proteases labeled in 0- to 5-dpf embryos. Immunoprecipitation with protein-specific antibodies identified the ABP-reactive proteins cathepsin L (Ctsl) and Z (Ctsz). For Ctsl and Ctsz, immunoprecipitation yielded single bands of similar molecular weight (MW) (Figure 2A). Although immunoprecipitation of Ctss yielded a 16-kDa band (the predicted MW of mature protease), several other Cy5-reactive bands were also pulled down (Figure S1A). The validity of these bands was assessed with a second ABP (BMV157) that predominantly recognizes Ctss (Oresic Bender et al., 2015). Both BMV109- and BMV157 labeled the 16-kDa band (mature Ctss) noted in immunoprecipitated samples (Figure 2B). Both probes also labeled one higher band, likely corresponding to a less processed form of mature Ctss. For Ctsk, a previously validated morpholino was used to reduce *ctsk* expression in developing embryos (Petrey et al., 2012). Comparison of BMV109-labeled WT and *ctsk* morphant embryos highlighted a 26-kDa protein that was specifically reduced following morpholino knockdown (Figure 2C). Reactivity with this band was also reduced when BMV109 was co-injected with the Ctsk-specific inhibitor odanacatib (Gauthier et al., 2008). These analyses established a set of MW standards for use in subsequent assays (Figure 2D). In-gel analyses of BMV109 reactivity in 0- to 5-day WT embryos revealed dynamic fluctuations in the activities of most bands (Figure 2E). Reactivity with the Ctsl/z band is fairly constant for the first 3 dpf but dramatically spikes 4 dpf and ultimately wanes 5 dpf. The spike in the Ctsl/z activity corresponds with a drastic reduction in Ctsk activity, which is typically undetectable by 4 dpf. In contrast, active Ctss increases substantially by 5 dpf.

Several Cts Activities Are Altered in MLII Embryos

Previous analyses with peptide-based substrates showed that Ctsk and Ctsl are increased in a zebrafish model of MLII (Petrey et al., 2012). To globally assess the degree to which these and other cathepsins are affected in MLII, we introduced BMV109 into WT and MLII embryos 0–4 dpf. BMV109 labeling showed minimal differences in protease activity between WT and MLII embryos 1 and 2 dpf (Figure 3A). By 3 dpf, however, the activity of Ctsl/z and Ctsk was increased in MLII (Figure 3B). Increases were sustained at 4 dpf, a time point when several WT activities (including Ctsk) typically wane (red arrow, Figure 3B). Quantitative analyses show that Ctsk and Ctsl/z activities are 50%–60% higher in MLII

embryos 2–3 dpf, with Ctsk nearly 100% higher 3–4 dpf (Figure 3C; Figure S1B). By 3 and 4 dpf, MLII embryos show a 40%–60% decrease in Ctss activity (green arrow, Figures 3B and 3C). Decreased activity is also noted with the Ctss probe BMV157 (Figure S1C). For all experiments, MLII embryos were generated using a previously validated morpholino to reduce *gnptab* expression (Flanagan-Steet et al., 2009). The BMV109 profiles noted in morphants were also confirmed in two different lines of stable transcription activator-like effector nuclease (TALEN)-generated *gnptab* knockout animals (Figure 3D). The details of this mutant are described elsewhere (unpublished data).

Confocal analyses of BMV109-labeled WT and MLII *fli1a*: EGFP-positive cartilages further showed several qualitative differences in cathepsin activity (Figure 3E). First, the majority of activity in WT tissues localized to discrete puncta in the mesenchyme adjacent to cartilage. In contrast, MLII embryos exhibited large irregular patches of activity found throughout chondrocytes and the mesenchyme. Second, magnified views showed several regions of cathepsin activity present outside of MLII (but not WT) cells (arrowheads, MLII-2, Figure 3E). This is consistent with our previous study, where enzymatic analysis of isolated cells showed that the majority of mature active Ctsk and Ctsl exists outside of MLII chondrocytes (Flanagan-Steet et al., 2016). In the present study, we utilized a transgenic line expressing a membrane-bound form of red fluorescent protein (*sox10*:mRFP) to confirm the extracellular location of BMV109- labeled activity (Figure 3F). Third, 3%–5% of WT chondrocytes exhibited a pericellular pattern of activity that was never seen in MLII cells (white arrowheads, WT, Figure 3E). This pattern is reminiscent of secretory lysosomes. Collectively, these data reveal several differences in the quantity and character of cathepsin activity in MLII.

TGF-β Signaling Increases Cts Activation

Previous analyses of MLII cartilage demonstrated that increased Ctsk is associated with abnormally high levels of TGF-β signaling (Flanagan-Steet et al., 2016). Inhibiting Ctsk restored normal TGF-β signaling and ameliorated MLII cartilage pathology. These data suggest that Ctsk acts upstream of TGF-β. Here we show that directly inhibiting TGF-β signaling also restores normal morphology to MLII cartilages. This is evident in Alcian blue-stained embryos treated from 3–4 dpf with either SB505124 (an Alk5/TgfβRI inhibitor) or losartan (an angiotensin II inhibitor that indirectly block activation of TGF-β ligands) (Figure 4A; Cohn et al., 2007; Habashi et al., 2006; Hagos et al., 2007; Ja wi ska et al., 2007). Pharmacological inhibition restored the shape and angle of articulation to several MLII structures, including the Meckel's (M) and ceratohyal (CH) cartilages. Detailed analyses of the degree of rescue can be found in Figure S2A.

To assess whether TGF-β inhibition exclusively exerts its restorative effect downstream of the cathepsins or whether drug treatment also reciprocally affects protease activity, BMV109 was injected into inhibitor-treated MLII embryos (schematic, Figure 4B). Surprisingly, TGF-β inhibition also reduced protease activity, with Ctsk being particularly sensitive to diminished TGF-β signals. Densitometry-based quantitation of individual bands showed that Ctsk activity was decreased 25%–30% in SB505124-treated MLII embryos and 45%–60% in losartan-treated embryos (Figure 4C). Analyses of phosphor-ylated Smads confirm that

activation of the TGF-β effector Smad2 declines in MLII embryos following drug treatment, whereas bone morphogenetic protein (BMP) effector (Smad1,5,8) activation increases (Figure 4B). Increased activation of Smad1,5,8 is consistent with the earlier demonstration that these two pathways are imbalanced in MLII, with TGF-β signaling high and BMP signaling low (Flanagan-Steet et al., 2016). The pSmad data indicate that TGF-β inhibition not only reduces Ctsk activity, but it also rebalances the TGF-β and BMP signaling cascades. Although prior analyses of Ctsk inhibition suggested that the protease acts upstream of TGF-β signaling, the fact that TGF-β inhibition also restores WT levels of Ctsk activity to MLII embryos indicates a reciprocal relationship between TGF-β and Ctsk.

To explore this further, we assessed whether manipulating TGF-β signaling in WT embryos also affects cathepsin activity. Unlike DMSO controls, treatment with either SB505124 or losartan reduced overall cathepsin activity (Figures 4D and 4E). However, treatment with the EGFR inhibitor erlotinib did not reduce probe reactivity with any protease (Figures S2B and S2C). The efficacy of all three inhibitors was evaluated by western blot of downstream effector activation. In WT treatment with erlotinib substantially reduced phospho-ERK levels, whereas addition of either SB505124 or losartan reduced phosphorylation of the TGF-β effector Smad2 without affecting phosphorylation of Smad1,5,8. Confocal analyses of TGF-β-inhibited WT and MLII embryos confirm that the decreased activity detected in-gel following SB505124 treatment corresponds to cartilage-localized changes in protease activity (Figures S2D and S2E). These data suggest a specific role for TGF-β-mediated regulation of cathepsin activity, a mode of action further supported by the fact that increasing TGF-β activation also increases cathepsin activity. This was shown using transgenic zebrafish that ex presses a constitutively active (CA) form of TgbrI controlled by the *hsp70* heat shock-responsive promoter (hsp70:CA*alk5*) (Figure 4F; see Figure S2F for the heat shock strategy). Although heat shock did not affect cathepsin activity in embryos lacking the CA*alk5* transgene, protease activity was increased 33% in transgenic embryos following heat shock (Figure 4G). Analyses of phosphorylated forms of the TGF-β effector Smad2 and the BMP effector Smad1,5,8 show that CAalk5 specifically enhanced TGF-β-propagated signals.

Ctsk Activity Is Post-translationally Regulated by TGF-β

To find out whether TGF-β signaling affects cathepsin expression, WT embryos were treated 3–4 dpf with losartan or SB505124, and transcript abundance was assessed 4 dpf by qRT-PCR (Figures 5 and S3A). Although inhibiting TGF-β signaling reduced the transcript levels of cathepsin B (*ctsba*) and one of the major isoforms of cathepsin L (*ctsl1b*) (Figure 5A), only the effects on ctsl1b were statistically significant. The transcript abundance of cathepsins H (*ctsh*), K (*ctsk*), S (*ctss1*), and Z (*ctsz*) was not affected by drug treatment (Figure 5B). The transcript abundance of *ctsba*, *h*, *k*, *s1*, and *z* was also unaffected when TGF-β signaling was inhibited in MLII embryos (Figure S3B). These data indicate that the TGF-β-mediated reductions in Ctsk activity may occur independent of changes in protease expression. To explore post-translational modes of regulation, we first analyzed Ctsk protein abundance across a developmental time course (Figures 5C–5E). This revealed several things about Ctsk processing *in vivo*. First, unlike the single intermediate noted by others *in vitro* (Lemaire et al., 2014), in developing tissue, we note multiple Ctsk forms. We detected

six high- and low-molecular-weight species in WT and MLII embryos 24 hpf. Second, although WT and MLII embryos express similar overall protein levels, they exhibit differences in the abundance of individual forms. In WT embryos, mature Ctsk (26 kDa) is present at 24 hpf, but, by 60 hpf, 65% of the enzyme is found in the inactive pro form (42 kDa) (Figure 5D; see Figures S4A–S4C for the quantitative method). This shift in form corresponds with the decreased activity noted in WT embryos at 3 dpf. In MLII embryos, not only is more Ctsk (80%) present in the mature form, this highly active species persists until 80 hpf (Figures 5C, 5E, and 5F and S4D).

The sustained abundance of mature Ctsk explains its heightened activity and also suggests that TGF-β may affect Ctsk by altering enzyme processing. To test this, WT and MLII embryos were treated at 50 hpf with SB505124. This time point was chosen because earlier treatments adversely affect heart development. Samples were harvested at multiple time points following drug addition (Figure 5G; Figures S4E–S4H). If the reduced activity noted following TGF-β inhibition were due to decreased Ctsk expression, then we would see less pro-Ctsk following drug addition. To the contrary, by 55 h, we typically detected more pro-Ctsk in drug-treated embryos. Increased levels of pro-enzyme were matched by a reduction in both the high-molecular-weight intermediate forms and the mature form of Ctsk (see enlarged gels and quantitation in Figures S4E–S4H). These data suggest that TGF-β signals regulate Ctsk activity by modulating enzymatic processing and activation.

C4-S Is Increased in MLII

Studies *in vitro* suggest that glycosaminoglycans (GAGs) modulate Ctsk activity (Lemaire et al., 2014; Li et al., 2000, 2004). In particular the 4-O-sulfated chains present on chondroitin sulfate proteoglycans (C4-S) can promote autocatalytic conversion of Ctsk to its mature form (Lemaire et al., 2014; Li et al., 2004). *chst11*, *12*, *13*, and *14* all encode sulfotransferases that synthesize C4-S, which is highly expressed during early chondrogenesis (Filipek-Górniok et al., 2013; Hayes et al., 2013; Holmborn et al., 2012). TGF-β has also been shown to stimulate *chst11* expression in cultured cells (Bhattacharyya et al., 2015; Susarla et al., 2011; Tiedemann et al., 2005). To find out whether differences in C4-S could explain MLII-associated increases in Ctsk processing and activity, we first assessed the transcript abundance of *chst11*, *12*, *13*, and *14* as well as the 6-O sulfated chondroitin (C6-S) sulfotransferases *chst3a* and *3b* and the C4-S sulfatase arylsulfatase B (*arsb*). Analyses of embryos 4 dpf demonstrate that, in MLII, the increased abundance of mature Ctsk is associated with more *chst11*, *13*, and *14* mRNA (Figure 6A). *chst12* mRNA was not detected 4 dpf. The transcript abundance of the C6-S sulfotransferases *chst3a* and *3b* and the C4-S sulfatase arylsulfatase B (*arsb*) was also slightly (but not always significantly) altered in MLII embryos (Figure S5A; Figure 6A). Inhibiting TGF-β signaling in MLII embryos with SB505124 3–4 dpf significantly reduced the transcript abundance of *chst11*, *13*, and *14* as well as *arsb* (Figure 6A). In WT embryos, TGF-β inhibition only significantly reduced *chst11* transcript abundance.

Increased *chst11* enzyme expression was confirmed by western blot, which showed that Chst11 levels are not only higher in MLII from 2–4 days but also reduced following TGF-β inhibition (Figure 6B). Confocal analyses of *fli1a*:EGFP-positive cartilage stained

immunohistochemically for C4-S suggest that MLII chondrocytes also express more C4-S than WT chondrocytes. Further, as noted with both chst11 transcript and protein, addition of SB505124 to either WT or MLII *fli1a*:EGFP embryos reduced C4-S staining (Figures 6C; and S5B). Immunohisto-chemical analyses of additional GAGs show that, unlike C4-S, the abundance of C6-S is reduced in MLII, whereas heparan sul-fate (HS) abundance is unaffected (Figures S5C and S5D). These findings indicate that elevated Ctsk activity present in MLII cartilage may correspond to TGF-β-regulated increases in C4-S.

To find out whether 4-O sulfated chondroitin is indeed increased in MLII embryos or, alternatively, whether C4-S staining reflects differences in antibody access, we used strong anion exchange high pressure liquid chromatography (SAX HPLC) to quantitatively assess GAG content in 4-day-old embryos. These analyses showed that C4-S normally constitutes 29% of total chondroitin sulfate (CS) (Figures 6D and 6E). Although the overall disaccharide weight was reduced by 33% in MLII, the relative level of C4-S to other forms of CS was globally increased 4%–5% (Figures 6E and S5E). This was matched by a 7% decrease in C6-S. The immunohistochemical data suggest that the bulk of increased C4-S may occur in craniofacial chondrocytes.

Inhibiting C4-S Synthesis Reduces Ctsk Activity and Improves MLII Phenotypes

The Chst11 sulfotransferase is considered the major C4-S-synthesizing enzyme (Klüppel, 2010; Klüppel et al., 2005). *In situ* analyses of sulfotransferase expression indicate Chst11 is the dominant form in developing zebrafish (Habicher et al., 2015). To functionally address the effect of C4-S on cathepsin activity, we inhibited *chst11* in WT and MLII embryos using a previously validated morpholino (Mizumoto et al., 2009). Western blot analyses show that 0.6 ng morpholino reduces Chst11 expression in WT and MLII embryos (Figures 7A and S6A and S6B). Immunohistochemical analyses confirm that *chst11* inhibition also reduces C4-S in GFP-positive chondrocytes (Figures 7B and S5B). In-gel analyses of BMV109-injected embryos show that *chst11*-inhibition also significantly reduces Ctsk activity. Reducing *chst11* expression lowered Ctsk activity 50% in MLII and WT embryos (Figures 7C and 7D) but only minimally affected Ctsl/z activity. Confocal analyses of BMV109 reactivity show that reduced Ctsk activity corresponds with chondrocyte-localized decreases in protease activity (Figures 7E and S2D and S2E). As expected, this is most evident in *chst11*-inhibited MLII cartilages. *chst11* inhibition also improved MLII craniofacial phenotypes (Figure 7F). Alcian blue-stained craniofacial cartilage show that *chst11* inhibition restores the shape and angle of articulation of the Meckel's and ceratohyal cartilages in 21% of MLII embryos (see details of the rescue in Figure S2A). As expected, 55% of *chst11*-inhibited WT embryos also exhibit alterations in these same cartilages (Figure 7F). These data show that *chst11*-driven C4-S synthesis affects Ctsk activity during both WT and MLII chondrogenesis.

chst11 Inhibition Impairs Ctsk Processing

To confirm that *chst11* inhibition reduces Ctsk activity by altering enzyme processing, Ctsk protein was analyzed in *chst11*-inhibited embryos (Figures 7G and 7H). Although the full range of Ctsk bands was present in *chst11*-inhibited embryos 24 hpf, by 36 hpf, we primarily detected the pro and mature forms. Uninjected samples exhibited very little pro-Ctsk

between 36 and 52 hr, suggesting that *chst11*-inhibition indeed impairs the initial steps of Ctsk processing (Figures 7G and 7H and S7). The abundance of mature Ctsk was also reduced following *chst11* inhibition, most notably in *chst11*-inhibited MLII embryos (Figures 7H and S7).

chst11 Inhibition Reduces TGF-β Signaling in MLII Cartilages

Several studies indicate that sulfated GAGs regulate growth factor bioavailability in developing tissues (Nandini and Sugahara, 2006). It was therefore unclear whether Chst11's effect on MLII cartilage pathology involved its ability to directly affect TGF-β signaling or whether synergy between Chst11-increased C4-S and Ctsk activation collectively stimulates signaling. To address this, we used an Smad binding element (SBE):nucCherry transgenic line that expresses nuclear mCherry in response to TGF-β signaling and assessed pathway activation under various conditions (Figures 7J and S7G). We asked whether inhibiting either *ctsk* or *chst11* expression similarly effected signaling in the WT and MLII backgrounds. As expected, treatment with SB505124 reduced the accumulation of nuclear localized Cherry in WT and MLII chondrocytes. *chst11* inhibition, however, had opposing effects on signaling in WT and MLII cartilages. Reducing C4-S abundance increased nuclearly localized Cherry expression in WT chondrocytes but reduced it in MLII cells. If C4-S GAGs only function to sequester TGF-β, then reducing C4-S should also enhance TGF-β signaling in MLII. *chst11* inhibition also decreased Ctsk activity in MLII, implying that Chst11 may also indirectly affect TGF-β by modulating Ctsk activity. The fact that direct inhibition of *ctsk* also reduced TGF-β signaling supports this (Figures 7J and S7G). Because morpholino inhibition of *chst11* and *ctsk* does not fully eliminate their expression, the degree to which each enzyme independently controls TGF-β signaling during normal chondrogenesis is currently not clear.

DISCUSSION

Cysteine cathepsins have emerged as important regulators of numerous biological processes (Reiser et al., 2010). Prior studies in zebrafish demonstrated a central role for extracellular Ctsk and enhanced TGF-β signaling in MLII cartilage pathology (Flanagan-Steet et al., 2016). This work suggests that extracellular Ctsk liberates TGF-β from latent complexes, sustaining its activity and impairing chondrogenesis. It further shows that Ctsk secretion is linked to its activation. Here we leverage an ABP to track cathepsins in normal and MLII zebrafish. We confirm that loss of lysosomal targeting alters cathepsin activity and uncover a regulatory mechanism whereby increased TGF-β signaling stimulates Ctsk activation. The data support a model in which TGF-β signals enhance the proteolytic processing of pro-Ctsk by modulating expression of C4-S-bearing GAGs. Increased Ctsk activation, in turn, drives sustained TGF-b signaling, creating a positive feedback loop that disrupts chondrogenesis (see Figure 7K for a model). Pharmacological intervention either at the level of Ctsk activity or TGF-β signaling short-circuits this loop, normalizing disease phenotypes. Prior studies have demonstrated that C4-S is highly expressed during early chondrogenesis, modulated by the TGF-β pathway (Carrino et al., 1983; Lincoln et al., 2006), and essential for Ctsk to degrade triple-helical collagen (Li et al., 2000, 2002, 2004). When combined with our data, this suggests that local GAG composition regulates Ctsk function in developing cartilage.

Altered cathepsin activity is implicated in the pathology of many lysosomal and non-lysosomal diseases (Bernstein et al., 1996; Bigg et al., 2013; Haque et al., 2008; Hua and Nair, 2015; Ketterer et al., 2017; Liu et al., 2004; Lutgens et al., 2007; Nixon, 2000; Vasiljeva et al., 2007; Wilson and Brömme, 2010). Because disrupted GAG profiles also characterize several lysosomal disorders, GAG-mediated differences in cathepsin activity could explain variability in bone and cartilage phenotypes. In mucopolysaccharidoses type I (MPSI), excessive buildup of HS and dermatan sulfate may reduce cathepsin K activity and inhibit collagen turnover, causing impaired osteoclast function, decreased cartilage resorption, and bone disease (Wilson and Brömme, 2010; Wilson et al., 2009). Conversely, as demonstrated in MLII zebrafish, increased chondroitin sulfate expression enhances the activity of extracellular cathepsin K. If operational in the bones of MLII patients, then increased cathepsin K activity could accelerate bone turnover, causing bone degeneration. Notably, the present work in MLII embryos also demonstrated decreased activity of cathepsin S. Unlike cathepsin K, C4-S is proposed to inhibit processing of pro cathepsin S, perhaps adversely affecting its function in S-expressing tissues, like macrophages or heart valves (Sage et al., 2013). Together, these findings reinforce the idea that disease-associated changes in GAG structure profoundly influence the activity and function of cysteine cathepsins, driving different phenotypic outcomes in developing tissue. The ability to faithfully monitor cathepsin proteases using ABPs provides numerous opportunities to study these important regulators of pathogenesis.

EXPERIMENTAL PROCEDURES

Zebrafish Strains and Husbandry

Animals were maintained according to standard protocols. Zebrafish strains were obtained from the Zebrafish International Resource Center (ZIRC, Eugene, OR) (TL, AB, and *Tg(fli1a:EGFP)y1* (Lawson and Weinstein, 2002). The *hsp70*:CA*alk5* strain was kindly provided by Dr. Caroline Burns (Harvard Medical School) (Zhou et al., 2011). The SBE:nucCherry TGF-β reporter line was kindly provided by Dr. Enrico Moro (Moro et al., 2013). All experiments were performed on synchronized populations, with collections and treatments performed at the same time point (i.e., 3 days = 72 hpf). To achieve this, fertilized eggs were recovered from mating chambers at 9 a.m. and immediately staged, and age-matched embryos were collected. Embryo age was reassessed the following day, and the 24 hpf (1 dpf) time point was assigned. Embryonic staging was performed according to established criteria (Kimmel et al., 1995). In some cases, 0.003% 1-phenyl 2-thiourea (PTU) was added to embryo medium to block pigmentation. Handling and euthanasia of fish for all experiments complied with the University of Georgia policies, as approved by the University of Georgia (UGA) Institutional Animal Care and Use Committee (permit A2015-07-003-A2).

BMV109 Delivery and Embryo Labeling

For all experiments, embryos were staged and synchronized by age within the first several hours and again before 24 hpf. The BMV109 ABP was injected into embryos at the time points indicated. Unless otherwise noted, 1 nL of a 10 μM solution of probe was introduced pericardially via microinjection. For the egg stage and younger embryos, this equates to a

final global concentration of 10 nM. Local concentration in specific tissues is unclear. Unless otherwise noted, the probe was circulated overnight at the normal growth temperature(28.8°C), and embryos were harvested 15 h post-injection. Exceptions to this (i.e., labeling followed by heat shock) are indicated in the Results and figure legends.

In-gel Analyses of BMV109 Reactivity

Embryos were dechorionated and the yolks manually removed at the stages indicated. 25 embryos per condition were collected and lysed in citrate buffer (50 mM citrate buffer [pH 5.5], 5 mM DTT, 0.5% 3-(3-cholamidopropyl) dimethylammonio)-1-propanesulfonate (CHAPS), and 0.75% Triton X-100) by brief sonication. Samples were centrifuged for 15 min at $15,000 \times g$, and the supernatant was collected. Protein concentration was determined via a micro-bicinchoninic acid (BCA) assay (catalog no. 23235, Thermo Fisher Scientific, Rockford, IL), and samples were run on 4%–20% precast gradient gels containing the "stain-free" tri-halo compound (Bio-Rad). UV light-activated tri-halo covalently binds tryptophan residues. Equivalent protein loads were evaluated on a Bio-Rad Chemidoc MP imaging system using this stain-free method. BMV109 Cy5 fluorescence was subsequently analyzed in-gel. Total protein load per lane and individual ABP-reactive bands were quantitated using Chemidoc MP software. Individual ABP-reactive bands were normalized to total protein load, and the fold difference was calculated between WT and MLII samples. Gel images were processed with Adobe Photoshop (CS6 extended, version 13.0).

Western Blot Analyses

Embryos were manually deyolked and harvested at the time points indicated. Western blot analyses for Ctsk were performed as described previously (Petrey et al., 2012). The western blots for pSmad2 and pSmad1,5,8 were blocked with 1% polyvinylpyrrolidone (PVP), followed by a 2-day incubation with the appropriate primary antibody (pSmad2 at 1/500, catalog no. 8828, Cell Signaling Technology; pSmad1,5,8 at 1/500, catalog no. 9511, Cell Signaling Technology). The western blots of Chst11 were performed using a zebrafish-specific antibody (1:1,000, catalog no. PA5–72647, Thermo Fisher Scientific, Rockford, IL). The blots were developed using the Bio-Rad Clarity substrate as directed and analyzed using the Bio-Rad MP Chemidoc system.

Statistical Analyses

In cases where numerical or quantitative data were generated, SD and a two-tailed Student's t test were used to assess statistical significance. Data were processed with GraphPad Prism (version 7.0a). In cases where staining patterns were assessed visually, representative embryos are shown, and the number of animals from multiple experimental samples that resembled those pictured was calculated. Embryo gender is not established until later in development; it is not a relevant consideration for these studies.

Additional methods (including use of morpholinos, pharmacological treatments, immunoprecipitations, and immunohistochemical analyses) are provided in the Supplemental Experimental Procedures.

Supplementary Material

Refer to Web version on PubMed Central for supplementary material.

ACKNOWLEDGMENTS

REFERENCES

Bernstein HG, Kirschke H, Wiederanders B, Pollak KH, Zipress A, and Rinne A (1996). The possible place of cathepsins and cystatins in the puzzle of Alzheimer disease: a review. Mol. Chem. Neuropathol 27, 225–247. [PubMed: 9147410]

Bhattacharyya S, Feferman L, and Tobacman JK (2015). Regulation of chondroitin-4-sulfotransferase (CHST11) expression by opposing effects of arylsulfatase B on BMP4 and Wnt9A. Biochim. Biophys. Acta 1849, 342–352. [PubMed: 25511584]

Bigg PW, Baldo G, Sleeper MM, O'Donnell PA, Bai H, Rokkam VR, Liu Y, Wu S, Giugliani R, Casal ML, et al. (2013). Pathogenesis of mitral valve disease in mucopolysaccharidosis VII dogs. Mol. Genet. Metab 110, 319–328. [PubMed: 23856419]

Carrino DA, Lennon DP, and Caplan AI (1983). Extracellular matrix and the maintenance of the differentiated state: proteoglycans synthesized by replated chondrocytes and nonchondrocytes. Dev. Biol 99, 132–144. [PubMed: 6617996]

Cohn RD, van Erp C, Habashi JP, Soleimani AA, Klein EC, Lisi MT, Gamradt M, ap Rhys CM, Holm TM, Loeys BL, et al. (2007). Angiotensin II type 1 receptor blockade attenuates TGF-beta-induced failure of muscle regeneration in multiple myopathic states. Nat. Med 13, 204–210. [PubMed: 17237794]

Edgington-Mitchell LE, Bogyo M, and Verdoes M (2017). Live Cell Imaging and Profiling of Cysteine Cathepsin Activity Using a Quenched Activity-Based Probe. Methods Mol. Biol 1491, 145–159. [PubMed: 27778287]

Filipek-Górniok B, Holmborn K, Haitina T, Habicher J, Oliveira MB, Hellgren C, Eriksson I, Kjellén L, Kreuger J, and Ledin J (2013). Expression of chondroitin/dermatan sulfate glycosyltransferases during early zebra-fish development. Dev. Dyn 242, 964–975. [PubMed: 23703795]

Flanagan-Steet H, Sias C, and Steet R (2009). Altered chondrocyte differentiation and extracellular matrix homeostasis in a zebrafish model for mucolipidosis II. Am. J. Pathol 175, 2063–2075. [PubMed: 19834066]

Flanagan-Steet H, Aarnio M, Kwan B, Guihard P, Petrey A, Haskins M, Blanchard F, and Steet R (2016). Cathepsin-Mediated Alterations in TGFβ-Related Signaling Underlie Disrupted Cartilage and Bone Maturation Associated With Impaired Lysosomal Targeting. J. Bone Miner. Res 31, 535–548. [PubMed: 26404503]

Gauthier JY, Chauret N, Cromlish W, Desmarais S, Duong LT, Falgueyret JP, Kimmel DB, Lamontagne S, Léger S, LeRiche T, et al. (2008). The discovery of odanacatib (MK-0822), a selective inhibitor of cathepsin K. Bioorg. Med. Chem. Lett 18, 923–928. [PubMed: 18226527]

Habicher J, Haitina T, Eriksson I, Holmborn K, Dierker T, Ahlberg PE, and Ledin J (2015). Chondroitin / dermatan sulfate modification enzymes in zebrafish development. PLoS One 10, e0121957. [PubMed: 25793894]

Habashi JP, Judge DP, Holm TM, Cohn RD, Loeys BL, Cooper TK, Myers L, Klein EC, Liu G, Calvi C, et al. (2006). Losartan, an AT1 antagonist, prevents aortic aneurysm in a mouse model of Marfan syndrome. Science 312, 117–121. [PubMed: 16601194]

Hagos EG, Fan X, and Dougan ST (2007). The role of maternal Activin-like signals in zebrafish embryos. Dev. Biol 309, 245–258. [PubMed: 17692308]

Haque A, Banik NL, and Ray SK (2008). New insights into the roles of endolysosomal cathepsins in the pathogenesis of Alzheimer's disease: cathepsin inhibitors as potential therapeutics. CNS Neurol. Disord. Drug Targets 7, 270–277. [PubMed: 18673211]

Hayes AJ, Reynolds S, Nowell MA, Meakin LB, Habicher J, Ledin J, Bashford A, Caterson B, and Hammond CL (2013). Spinal deformity in aged zebrafish is accompanied by degenerative changes to their vertebrae that resemble osteoarthritis. PLoS ONE 8, e75787. [PubMed: 24086633]

Holmborn K, Habicher J, Kasza Z, Eriksson AS, Filipek- Górniok B, Gopal S, Couchman JR, Ahlberg PE, Wiweger M, Spillmann D, et al. (2012). On the roles and regulation of chondroitin sulfate and heparan sulfate in zebrafish pharyngeal cartilage morphogenesis. J. Biol. Chem 287, 33905–33916. [PubMed: 22869369]

Honey K, and Rudensky AY (2003). Lysosomal cysteine proteases regulate antigen presentation. Nat. Rev. Immunol 3, 472–482. [PubMed: 12776207]

Hook V, Funkelstein L, Lu D, Bark S, Wegrzyn J, and Hwang SR (2008). Proteases for processing proneuropeptides into peptide neurotransmitters and hormones. Annu. Rev. Pharmacol. Toxicol 48, 393–423. [PubMed: 18184105]

Hua Y, and Nair S (2015). Proteases in cardiometabolic diseases: Pathophysiology, molecular mechanisms and clinical applications. Biochim. Biophys. Acta 1852, 195–208. [PubMed: 24815358]

Ja wi ska A, Badakov R, and Keating MT (2007). Activin-betaA signaling is required for zebrafish fin regeneration. Curr. Biol 17, 1390–1395. [PubMed: 17683938]

Kato D, Boatright KM, Berger AB, Nazif T, Blum G, Ryan C, Chehade KA, Salvesen GS, and Bogyo M (2005). Activity-based probes that target diverse cysteine protease families. Nat. Chem. Biol 1, 33–38. [PubMed: 16407991]

Ketterer S, Gomez-Auli A, Hillebrand LE, Petrera A, Ketscher A, and Reinheckel T (2017). Inherited diseases caused by mutations in cathepsin protease genes. FEBS J 284, 1437–1454. [PubMed: 27926992]

Kimmel CB, Ballard WW, Kimmel SR, Ullmann B, and Schilling TF (1995). Stages of embryonic development of the zebrafish. Dev. Dyn 203, 253–310. [PubMed: 8589427]

Klüppel M (2010). The roles of chondroitin-4-sulfotransferase-1 in development and disease. Prog. Mol. Biol. Transl. Sci 93, 113–132. [PubMed: 20807643]

Klüppel M, Wight TN, Chan C, Hinek A, and Wrana JL (2005). Maintenance of chondroitin sulfation balance by chondroitin-4-sulfotransferase 1 is required for chondrocyte development and growth factor signaling during cartilage morphogenesis. Development 132, 3989–4003. [PubMed: 16079159]

Kollmann K, Pohl S, Marschner K, Encarnação M, Sakwa I, Tiede S, Poorthuis BJ, Lübke T, Müller-Loennies S, Storch S, and Braulke T (2010). Mannose phosphorylation in health and disease. Eur. J. Cell Biol 89, 117–123. [PubMed: 19945768]

Kornfeld S, and Mellman I (1989). The biogenesis of lysosomes. Annu. Rev. Cell Biol 5, 483–525. [PubMed: 2557062]

Lawson ND, and Weinstein BM (2002). In vivo imaging of embryonic vascular development using transgenic zebrafish. Dev. Biol 248, 307–318. [PubMed: 12167406]

Lemaire PA, Huang L, Zhuo Y, Lu J, Bahnck C, Stachel SJ, Carroll SS, and Duong LT (2014). Chondroitin sulfate promotes activation of cathepsin K. J. Biol. Chem 289, 21562–21572. [PubMed: 24958728]

Li Z, Hou WS, and Brömme D (2000). Collagenolytic activity of cathepsin K is specifically modulated by cartilage-resident chondroitin sulfates. Biochemistry 39, 529–536. [PubMed: 10642177]

Li Z, Hou WS, Escalante-Torres CR, Gelb BD, and Bromme D (2002). Collagenase activity of cathepsin K depends on complex formation with chondroitin sulfate. J. Biol. Chem 277, 28669–28676. [PubMed: 12039963]

Li Z, Yasuda Y, Li W, Bogyo M, Katz N, Gordon RE, Fields GB, and Brömme D (2004). Regulation of collagenase activities of human cathepsins by glycosaminoglycans. J. Biol. Chem 279, 5470–5479. [PubMed: 14645229]

Lincoln J, Lange AW, and Yutzey KE (2006). Hearts and bones: shared regulatory mechanisms in heart valve, cartilage, tendon, and bone development. Dev. Biol 294, 292–302. [PubMed: 16643886]

Liu J, Sukhova GK, Sun JS, Xu WH, Libby P, and Shi GP (2004). Lysosomal cysteine proteases in atherosclerosis. Arterioscler. Thromb. Vasc. Biol 24, 1359–1366. [PubMed: 15178558]

Lutgens SP, Cleutjens KB, Daemen MJ, and Heeneman S (2007). Cathepsin cysteine proteases in cardiovascular disease. FASEB J 21, 3029–3041. [PubMed: 17522380]

Mizumoto S, Mikami T, Yasunaga D, Kobayashi N, Yamauchi H, Miyake A, Itoh N, Kitagawa H, and Sugahara K (2009). Chondroitin 4-O-sulfotransferase-1 is required for somitic muscle development and motor axon guidance in zebrafish. Biochem. J 419, 387–399. [PubMed: 19125692]

Moro E, Vettori A, Porazzi P, Schiavone M, Rampazzo E, Casari A, Ek O, Facchinello N, Astone M, Zancan I, et al. (2013). Generation and application of signaling pathway reporter lines in zebrafish. Mol. Genet. Genomics 288, 231–242. [PubMed: 23674148]

Nandini CD, and Sugahara K (2006). Role of the sulfation pattern of chondroitin sulfate in its biological activities and in the binding of growth factors. Adv. Pharmacol 53, 253–279. [PubMed: 17239770]

Nixon RA (2000). A "protease activation cascade" in the pathogenesis of Alzheimer's disease. Ann. N Y Acad. Sci 924, 117–131. [PubMed: 11193788]

Olson OC, and Joyce JA (2015). Cysteine cathepsin proteases: regulators of cancer progression and therapeutic response. Nat. Rev. Cancer 15, 712–729. [PubMed: 26597527]

Oresic Bender K, Ofori L, van der Linden WA, Mock ED, Datta GK, Chowdhury S, Li H, Segal E, Sanchez Lopez M, Ellman JA, et al. (2015). Design of a highly selective quenched activity-based probe and its application in dual color imaging studies of cathepsin S activity localization.J. Am. Chem. Soc 137, 4771–4777. [PubMed: 25785540]

Petrey AC, Flanagan-Steet H, Johnson S, Fan X, De la Rosa M, Haskins ME, Nairn AV, Moremen KW, and Steet R (2012). Excessive activity of cathepsin K is associated with cartilage defects in a zebrafish model of mucolipidosis II. Dis. Model. Mech 5, 177–190. [PubMed: 22046029]

Reiser J, Adair B, and Reinheckel T (2010). Specialized roles for cysteine cathepsins in health and disease. J. Clin. Invest 120, 3421–3431. [PubMed: 20921628]

Reitman ML, Varki A, and Kornfeld S (1981). Fibroblasts from patients with I-cell disease and pseudo-Hurler polydystrophy are deficient in uridine 5′-diphosphate-N-acetylglucosamine: glycoprotein N-acetylglucosaminylphosphotransferase activity. J. Clin. Invest 67, 1574–1579. [PubMed: 6262380]

Sage J, Mallèvre F, Barbarin-Costes F, Samsonov SA, Gehrcke JP, Pisabarro MT, Perrier E, Schnebert S, Roget A, Livache T, et al. (2013). Binding of chondroitin 4-sulfate to cathepsin S regulates its enzymatic activity. Biochemistry 52, 6487–6498. [PubMed: 23968158]

Sanman LE, and Bogyo M (2014). Activity-based profiling of proteases. Annu. Rev. Biochem 83, 249–273. [PubMed: 24905783]

Stoka V, Turk V, and Turk B (2016). Lysosomal cathepsins and their regulation in aging and neurodegeneration. Ageing Res. Rev 32, 22–37. [PubMed: 27125852]

Susarla BT, Laing ED, Yu P, Katagiri Y, Geller HM, and Symes AJ (2011). Smad proteins differentially regulate transforming growth factor-b-mediated induction of chondroitin sulfate proteoglycans. J. Neurochem 119, 868–878. [PubMed: 21895657]

Tiede S, Storch S, Lübke T, Henrissat B, Bargal R, Raas-Rothschild A, and Braulke T (2005). Mucolipidosis II is caused by mutations in GNPTA encoding the alpha/beta GlcNAc-1-phosphotransferase. Nat. Med 11, 1109–1112. [PubMed: 16200072]

Tiedemann K, Olander B, Eklund E, Todorova L, Bengtsson M, Maccarana M, Westergren-Thorsson G, and Malmström A (2005). Regulation of the chondroitin/dermatan fine structure by transforming growth factor-beta1 through effects on polymer-modifying enzymes. Glycobiology 15, 1277–1285. [PubMed: 16118286]

Vasiljeva O, Reinheckel T, Peters C, Turk D, Turk V, and Turk B (2007). Emerging roles of cysteine cathepsins in disease and their potential as drug targets. Curr. Pharm. Des 13, 387–403. [PubMed: 17311556]

Verdoes M, Oresic Bender K, Segal E, van der Linden WA, Syed S, Withana NP, Sanman LE, and Bogyo M (2013). Improved quenched fluorescent probe for imaging of cysteine cathepsin activity. J. Am. Chem. Soc 135, 14726–14730. [PubMed: 23971698]

Wilson S, and Brömme D (2010). Potential role of cathepsin K in the pathophysiology of mucopolysaccharidoses. J. Pediatr. Rehabil. Med 3, 139–146. [PubMed: 21629671]

Wilson S, Hashamiyan S, Clarke L, Saftig P, Mort J, Dejica VM, and Brömme D (2009). Glycosaminoglycan-mediated loss of cathepsin K collage nolytic activity in MPS I contributes to osteoclast and growth plate abnormalities. Am. J. Pathol 175, 2053–2062. [PubMed: 19834056]

Zhang D, Leung N, Weber E, Saftig P, and Brömme D (2011). The effect of cathepsin K deficiency on airway development and TGF-b1 degradation. Respir. Res 12, 72. [PubMed: 21627832]

Zhou Y, Cashman TJ, Nevis KR, Obregon P, Carney SA, Liu Y, Gu A, Mosimann C, Sondalle S, Peterson RE, et al. (2011). Latent TGF-b binding protein 3 identifies a second heart field in zebrafish. Nature 474, 645–648. [PubMed: 21623370]

Highlights

- Cathepsin activities are altered without carbohydrate-dependent lysosomal targeting

- TGF-β signaling controls cathepsin K activity at the level of enzyme processing

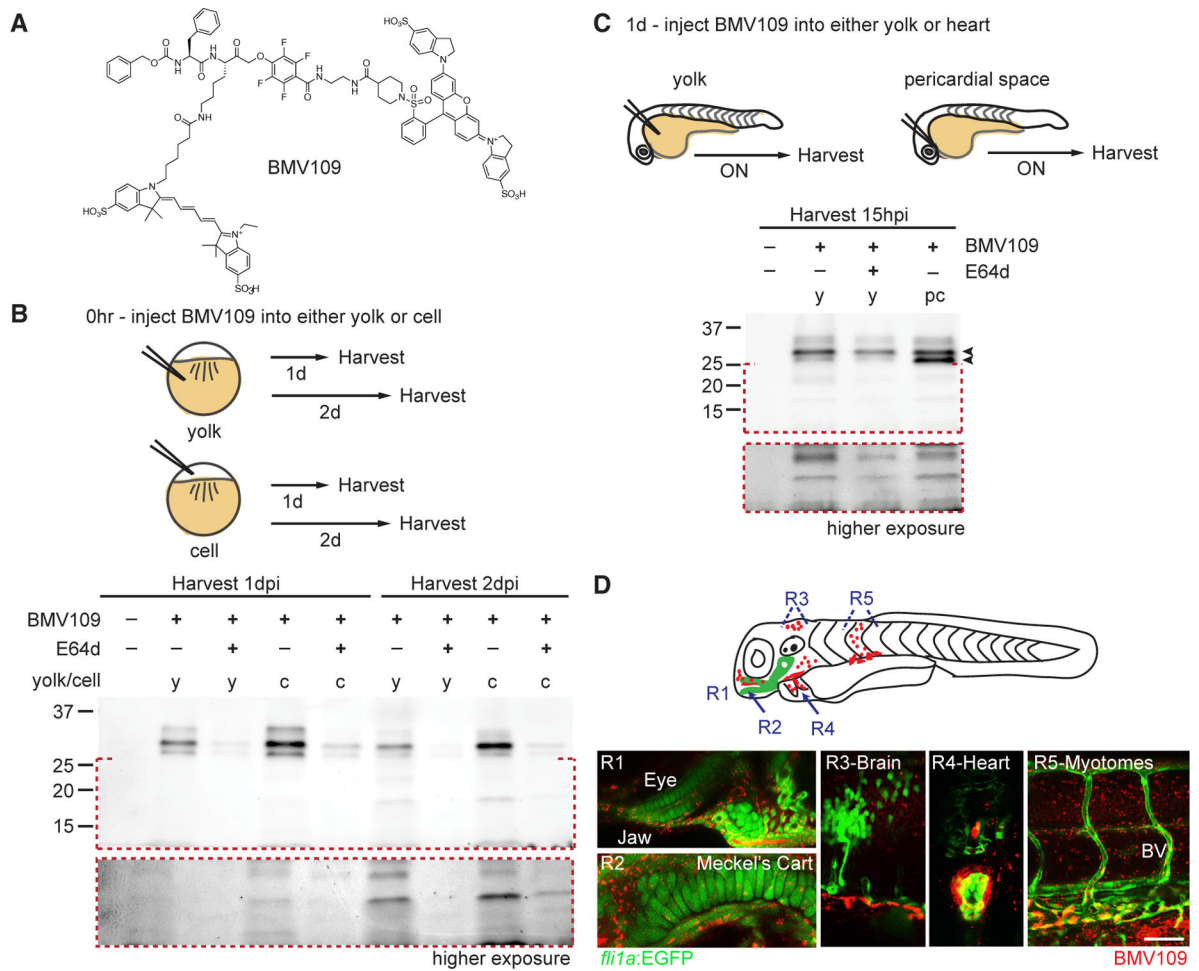- TGF-β promotes cathepsin K processing by enhancing expression of chondroitin-4-sulfate

Figure 1. BMV109 Labels Cathepsin Proteases in Developing Zebrafish

(A) BMV109 ABP structure.

(B) Schematic of injection strategies. Shown are in-gel analyses of BMV109 reactivity. The bottom gel panels (outlined in red) are higher exposures of low-molecular-weight species; n = 4 experiments. For all gels, equivalence of protein loaded per lane was confirmed using the stain-free method (Experimental Procedures).

(C) BMV109 was injected into the yolk or pericardial space of 1 dpf embryos and incubated overnight (15 hr); n = 4 experiments.

(D) Live confocal analyses of 4 dpf *fli1a*:EGFP-positive embryos injected pericardially with BMV109 (red, imaging done 15 hr post injection [hpi]). The schematic shows 5 regions (R1–R5) spanning multiple embryonic tissues oriented head to tail. Meckel's cartilage, lower jaw cartilage; BV, blood vessel. Scale bar, 10 μm. n = 30 embryos from 3 experiments. See also Figure S1.
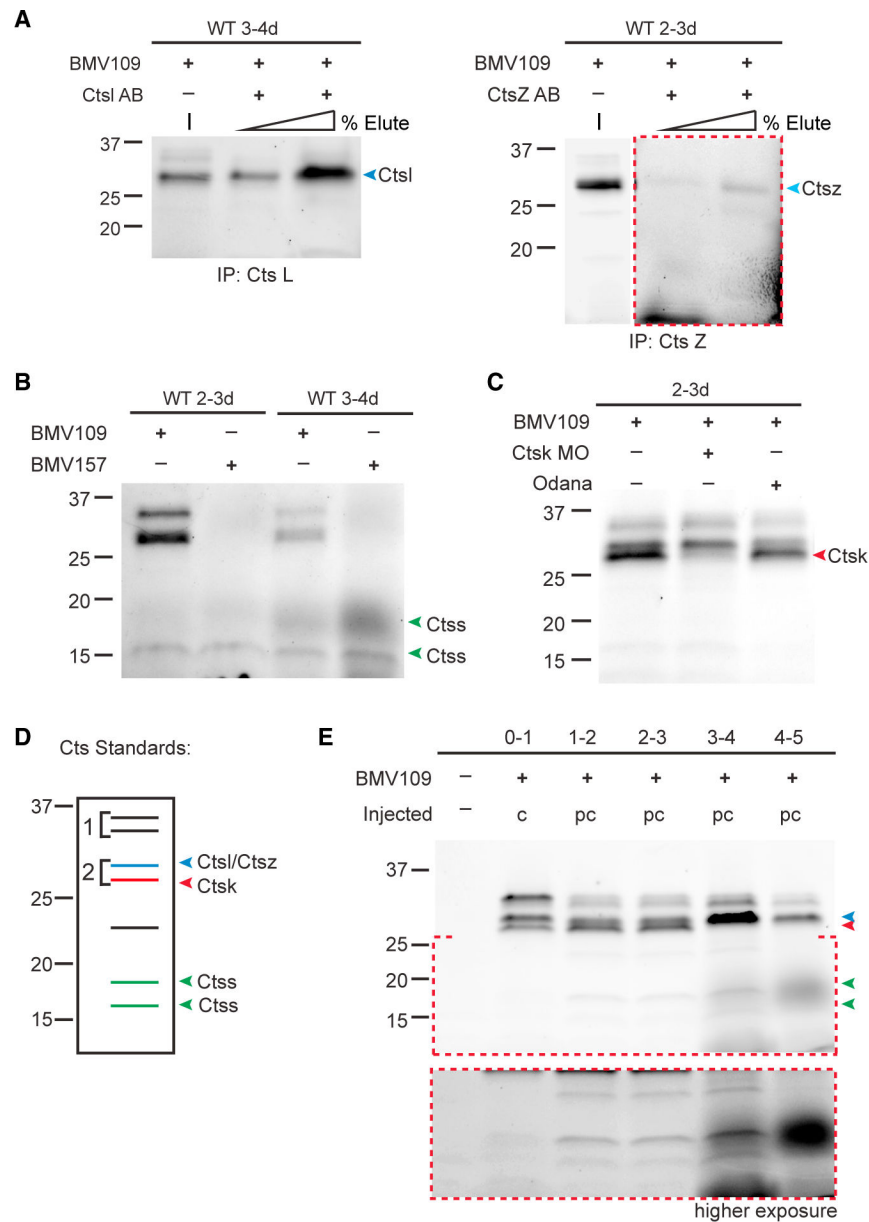
Figure 2. Biochemical Analyses Identify Cathepsin k, l, s, and z Bands

(A) Immunoprecipitation with antibodies for either Ctsl or Ctsz. Immunoprecipitated protein from two different loading concentrations (25% and 75% of total eluted protein, ▱) is shown. To avoid saturation, for Ctsz, the BMV109 input lane is shown at a lower exposure than eluted lanes (outlined in red). n = 4 experiments.

(B) 2 and 3 dpf embryos labeled overnight (15 hr) with either BMV109 or BMV157. n = 3 experiments.

(C) BMV109 in Ctsk-inhibited embryos. Ctsk expression was inhibited either by morpholino (MO) or the Ctsk inhibitor odanacatib (10 nM, Odana). n = 3 experiments.

(D) Schematic of BMV109-labeled cathepsins. Doublets 1 and 2 are highlighted.

(E) In-gel analyses of BMV109-labeled WT embryos. BMV109 was injected into the cell (c, 0–1 day) or heart (pericardial [pc], 1–5 days). The bottom gel (outlined in red) is a higher

exposure of the low-molecular-weight species. Colored arrowheads denote individual cathepsins (see schematic). n = 4 experiments. See also Figure S1.
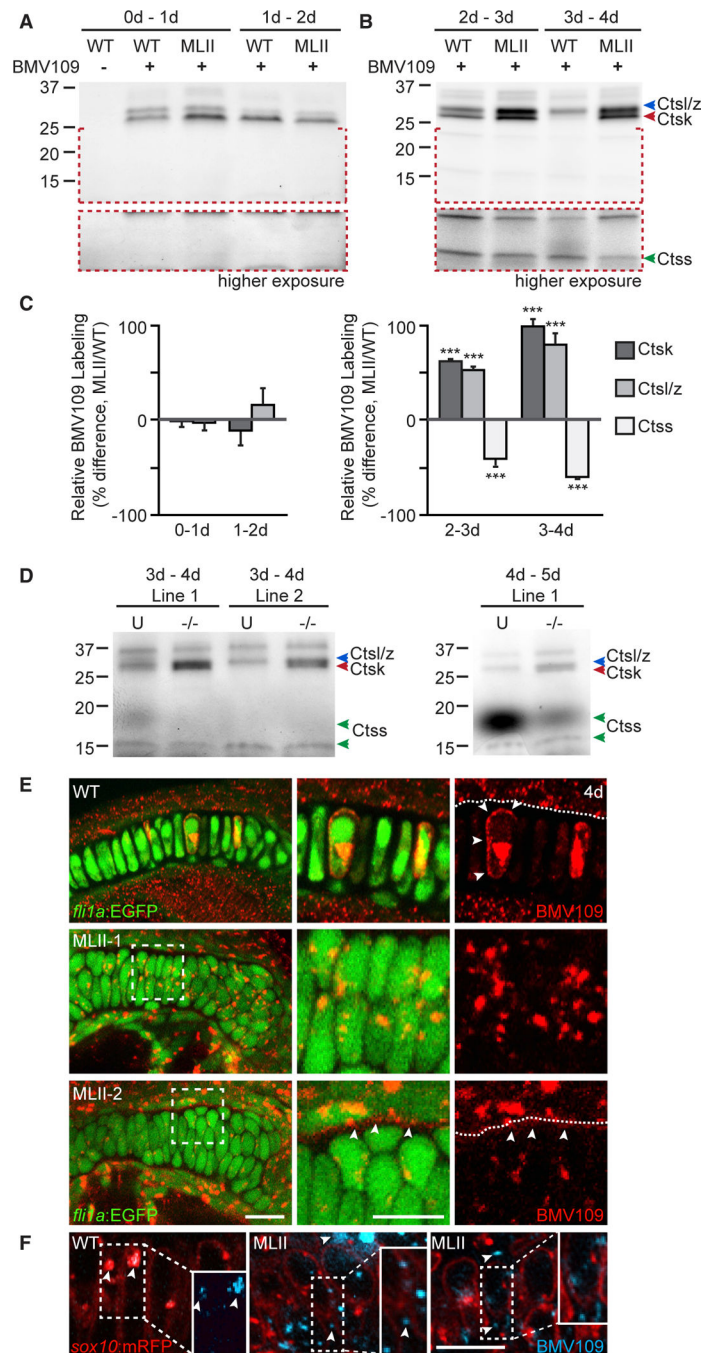
Figure 3. Cathepsin Activities Are Altered in MLII

(A) In-gel analyses show Cts activities in WT and MLII embryos 0–1 and 1–2 dpf. n = 4 experiments.

(B) Analyses of BMV109-labeled embryos 2–3 and 3–4 dpf. n = 4 experiments.

(C) Quantitation of the Ctsk, Ctsl/z, and Ctss bands from 4 experiments. Error bars, SD; ***p < 0.001. For all gels, the equivalence of total protein loaded per lane was evaluated using the stain-free method described in the Experimental Procedures.

(D) BMV109 labeling of *gnptab* TALEN-mediated stable knockout embryos 3–4 dpf. U, unaffected (*gnptab*^{+/+} and *gnptab*^{+/−} embryos); (−/−), *gnptab*^{−/−} from two null zebrafish lines. n = 3 experiments.

(E) Live confocal analyses of BMV109-labeled (red) *fli1a*:EGFP (green) WT and MLII embryos. White boxes indicate magnified views shown in the center (green and red) and at the right (red, BMV109). White arrows highlight pericellular puncta in WT and extra-cellular activity in MLII. Dotted lines demarcate cell boundaries. n = 15 embryos from 3 experiments.

(F) Live confocal analyses of BMV109-labeled activity (blue) in *sox10*:mRFP (red, membrane-bound) transgenic embryos. In the WT, BMV109 reactivity (blue) co-localizes with RFP-positive cellular regions (see RFP-negative inset, white arrows) but can be found extracellularly (white arrows) in MLII embryos. The insets represent magnified views of the boxed areas. Scale bars, 10 μm. See also Figure S1.
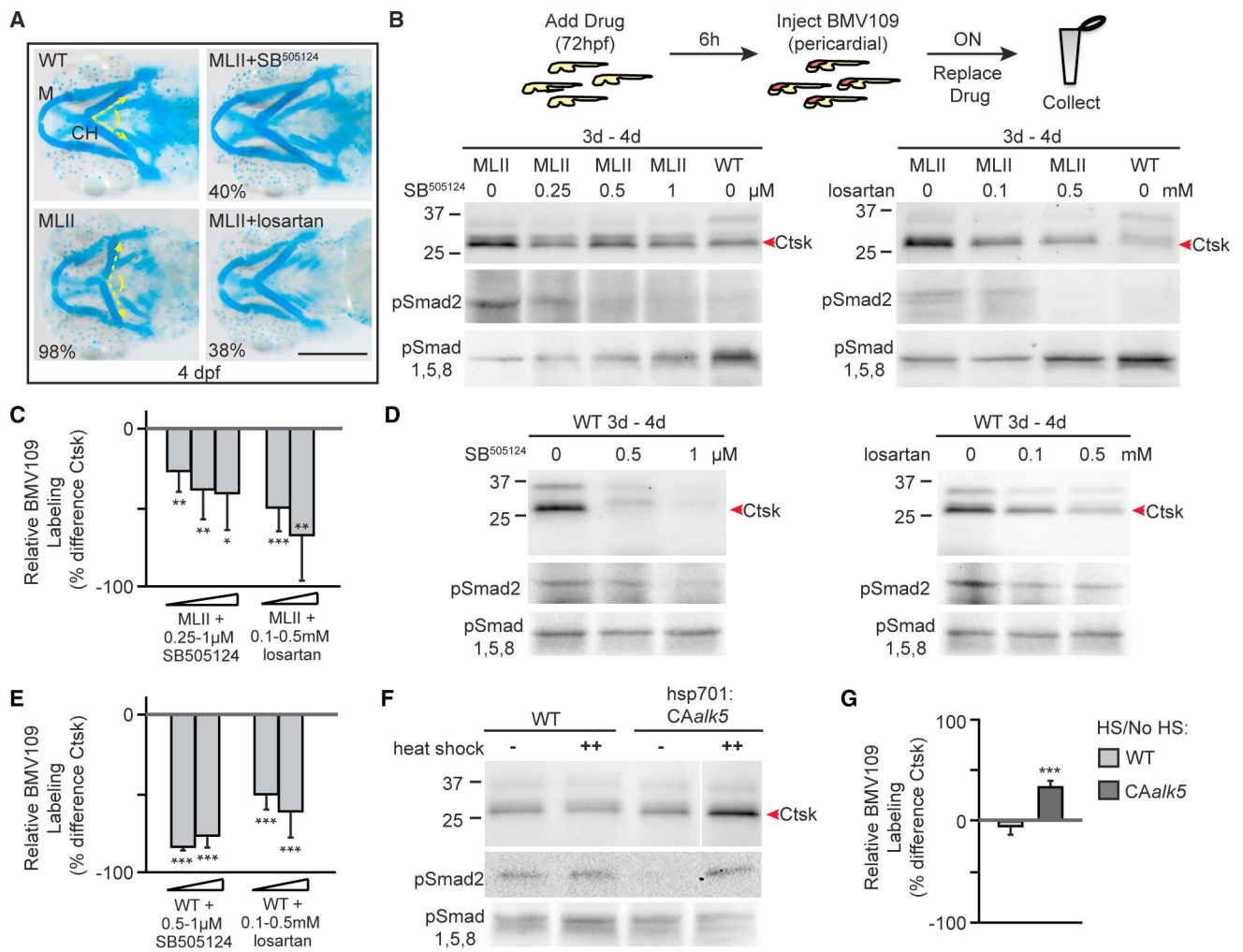
Figure 4. TGF-β Inhibition Ameliorates MLII Pathology and Reduces Ctsk Activity

(A) Alcian blue stains of 4 dpf WT, MLII, and TGF-β-inhibited embryos. Shown are Meckel's (M) cartilage and the angle of ceratohyal (CH) cartilages. The angle of cartilage articulation is illustrated by yellow dotted lines. Scale bar, 10 μm. Percent values are the number of embryos that resembled the picture (i.e., were rescued). n = 75–100 embryos from 3 experiments.

(B) Schematic illustrating the treatment regimen. Shown are in-gel analyses of BMV109 reactivity (top), immunoblots of phosphorylated pSmad2 (TGF-β effector, center), and phosphorylated pSmad1,5,8 (BMP effector, bottom). n = 4 experiments.

(C) Quantitation of BMV109-labeled Ctsk in treated and untreated MLII embryos from 4 experiments. Error bars, SD; *p < 0.05, **p < 0.01, ***p < 0.001.

(D) In-gel analyses of BMV109-labeled (top) WT embryos, immunoblots of phosphorylated pSmad2 (TGF-β effector, center), and phosphorylated pSmad1,5,8 (BMP effector, bottom). n = 4 experiments.

(E) Quantitation of BMV109-labeled Ctsk in treated and untreated WT embryos from 4 experiments.

(F) Gels of BMV109 labeling after TGF-β induction (top) and immunoblots for psmad2 and pSmad1,5,8 (bottom). n = 5 experiments.

(G) Quantitation of BMV109-labeled Ctsk before and after heat shock. Error bars, SD; ***p < 0.001. See also Figure S2.
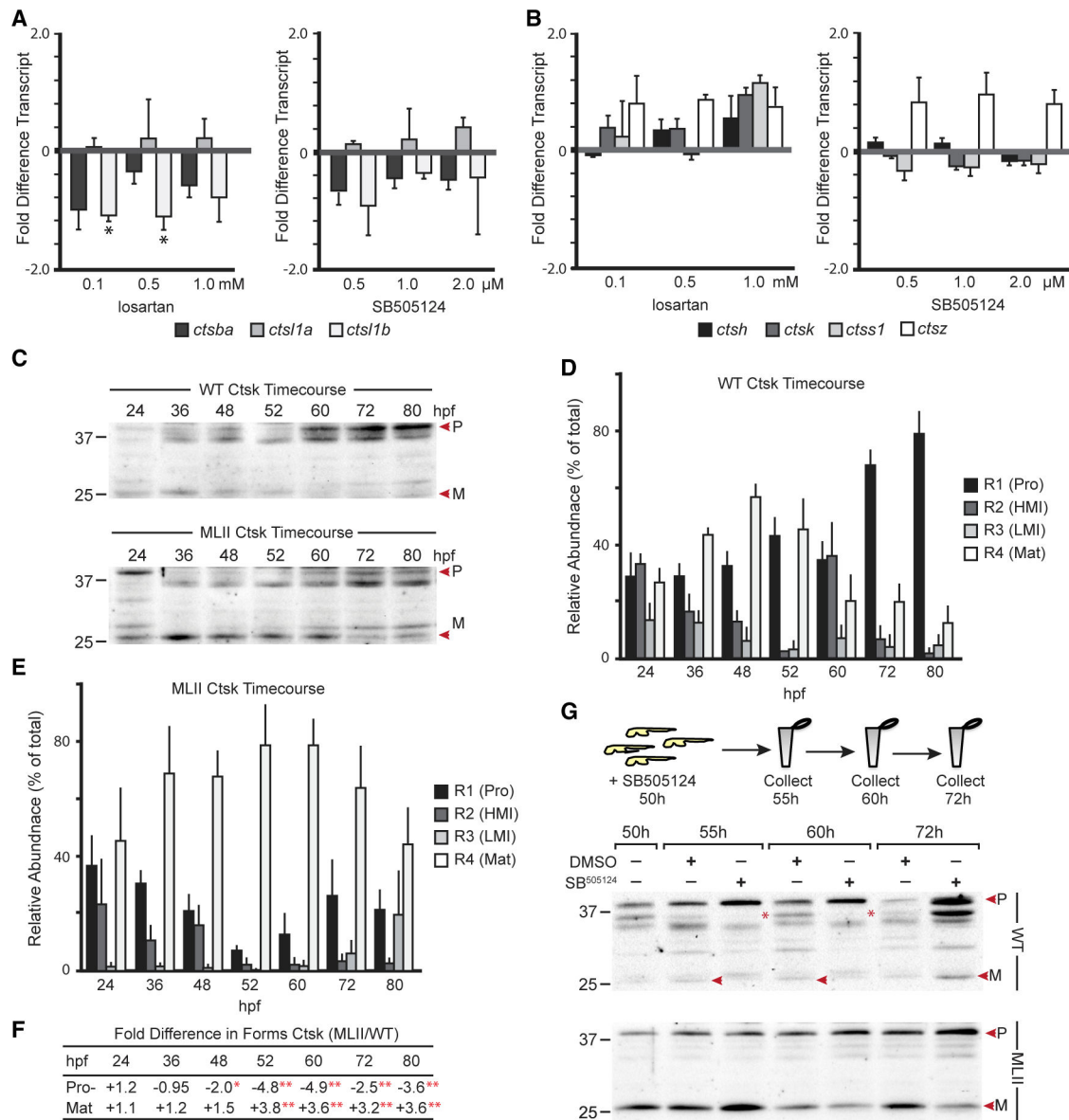
Figure 5. TGF-β Inhibition Impairs Ctsk Processing

(A) qRT-PCR of cathepsin B (*ctsba*), L1a, and L1b transcript abundance in 3–4 dpf WT embryos before and after TGF-β inhibition. Error bars, SD; *p < 0.05.

(B) qRT-PCR of cathepsin H, K, S (*ctss1*), and Z transcript abundance. Error bars, SD; n = 4 experiments of 25 embryos per condition.

(C) Immunoblots for Ctsk in WT and MLII embryos 24–80 hpf. Shown are pro (P; 42 kDa) and mature (M; 26 kDa) Ctsk forms.

(D and E) WT (D) and MLII (E) graphs presenting relative abundances of 4 regions (R1–R4; see Figure S4 for a full description) encompassing pro, intermediate (both high [HMI] and low [LMI] molecular weight intermediate), and mature forms of Ctsk in WT and MLII. n = 4 experiments. Error bars, SD.

(F) Table showing the fold difference of pro and mature forms 24–80 hpf from WT and MLII. *p < 0.05, **p < 0.01.

(G) Immunoblot of Ctsk in WT and MLII embryos following treatment with SB505124 (see the schematic for the treatment regimen). Red asterisks highlight intermediate forms. Red arrows on the gels indicate the mature form. See Figure S4 for quantitation. n = 4 independent experiments. See also Figures S3 and S4.
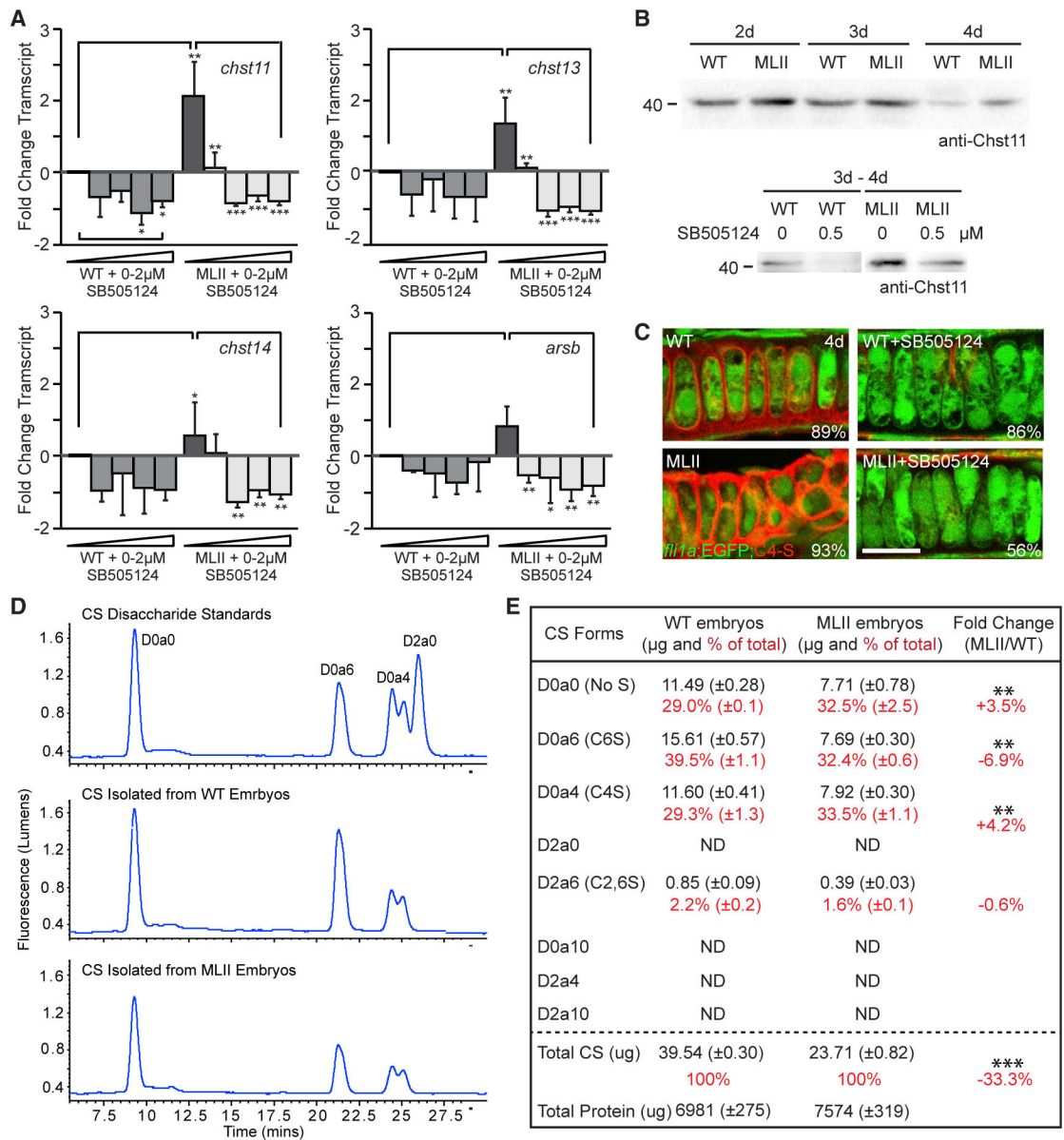
Figure 6. TGF-β-Mediated Regulation of C4-S Controls Ctsk Activity

(A) qRT-PCR of chondroitin-4-sulfate biosynthetic enzymes (*chst11*, *13*, and *14*) in TGF-β-inhibited WT and MLII embryos 4 dpf. n = 4 experiments. Error bars, SD; *p < 0.05, **p < 0.01, ***p < 0.001.

(B) Western blots of Chst11 in WT and MLII embryos 2–4 dpf and in TGF-β-inhibited embryos. n = 3 experiments. d, dpf.

(C) Immunohistochemistry of C4-S (red) in *fli1a*:EGFP WT and MLII cartilage sections. n = 15–20 embryos per condition from 3 experiments. Percent values are the number of embryos that resemble the picture. Scale bar, 10 μm.

(D and E) Traces of SAX HPLC for chondroitin sulfate forms in WT and MLII embryos (D). Table of SAX HPLC data (E). n = 3 technical replicates of 1 biological set with 1,200 embryos per sample. A second biological sample is presented in Figure S6. Error bars, SD;

**p < 0.01, ***p < 0.001. Standards for additional sulfo-forms, including C2,6S (D2a6), were also used. Because of their late elution time and low detection levels, these data were not included in the raw traces. See also Figure S5.

A WT

anti- Chst11

B WT / WT+*chst11* MO / MLII / MLII+*chst11* MO — *fli1a*:EGFP:C4-S

C 3-4d — ◄Ctsk / BMV109 — ◄Ctsk

D

E WT / MLII / WT+*chst11*^MO / MLII+*chst11*^MO — *fli1a*:EGFP / BMV109

F WT / MLII / WT+*chst11* MO / MLII+*chst11* MO — CH, M

G Ctsk Timecourse WT embryos / *chst11*-inhibited WT embryos — ◄P, ◄M

H Ctsk Timecourse MLII embryos / *chst11*-inhibited MLII embryos — ◄P, ◄M

K Cathepsin K Activated — stimulate / Inhibit? — C4-S GAGs on CSPG / H2-S GAGs on HSPG — TGFß Signaling / BMP Signaling — *chst11*↑ — abnormal chondrogenesis

I

Age (hpf)	WT Pro	WT Mat	WT+*chst11* MO Pro	WT+*chst11* MO Mat	Fold Δ (+/-) Pro	Fold Δ (+/-) Mat	MLII Pro	MLII Mat	MLII+*chst11* MO Pro	MLII+*chst11* MO Mat	Fold Δ (+/-) Pro	Fold Δ (+/-) Mat
24	29±4.7	43±2.6	2±0.6	7±0.4	-15***	-6.4	37±11	47±2.6	6±4.1	10±3.8	-5.9***	-4.5***
36	33±5.3	58±4.0	36±6.4	46±8.1	+1.1	-1.3	31±5.0	70±17	38±10	18±3.7	+1.2	-3.9***
48	43±7.5	46±14	69±3.0	16±2.4	+1.6*	-2.8**	21±6.3	69±9.6	33±0.8	18±2.6	+1.5*	-3.8***
52	35±6.7	21±12	57±6.3	9±1.6	+1.6*	-2.4*	7±1.8	80±15	38±4.0	25±1.9	+5.2***	-3.2***
60	64±17	22±5.6	78±9.5	2±1.6	+1.2	-9.7***	13±8.7	80±9.9	35±1.5	13±5.3	+2.7**	-6.1***
72	68±5.6	20±6.3	42±8.6	3±1.1	-1.4	-7***	25±13.0	65±15	35±0.8	7±2.9	+1.4*	-9.3***
80	79±8.7	13±6.6	48±7.3	4±0.8	-1.5*	-3.4**	22±7.0	45±13	33±1.5	3±0.5	+1.5*	-16***
	% of total (R1-R4)						% of total (R1-R4)					

J WT / WT+SB^505124 / WT+chst11^MO / WT+ctsk^MO / MLII / MLII+SB^505124 / MLII+chst11^MO / MLII+ctsk^MO — *fli1a*:EGFP / SBE:mCherry
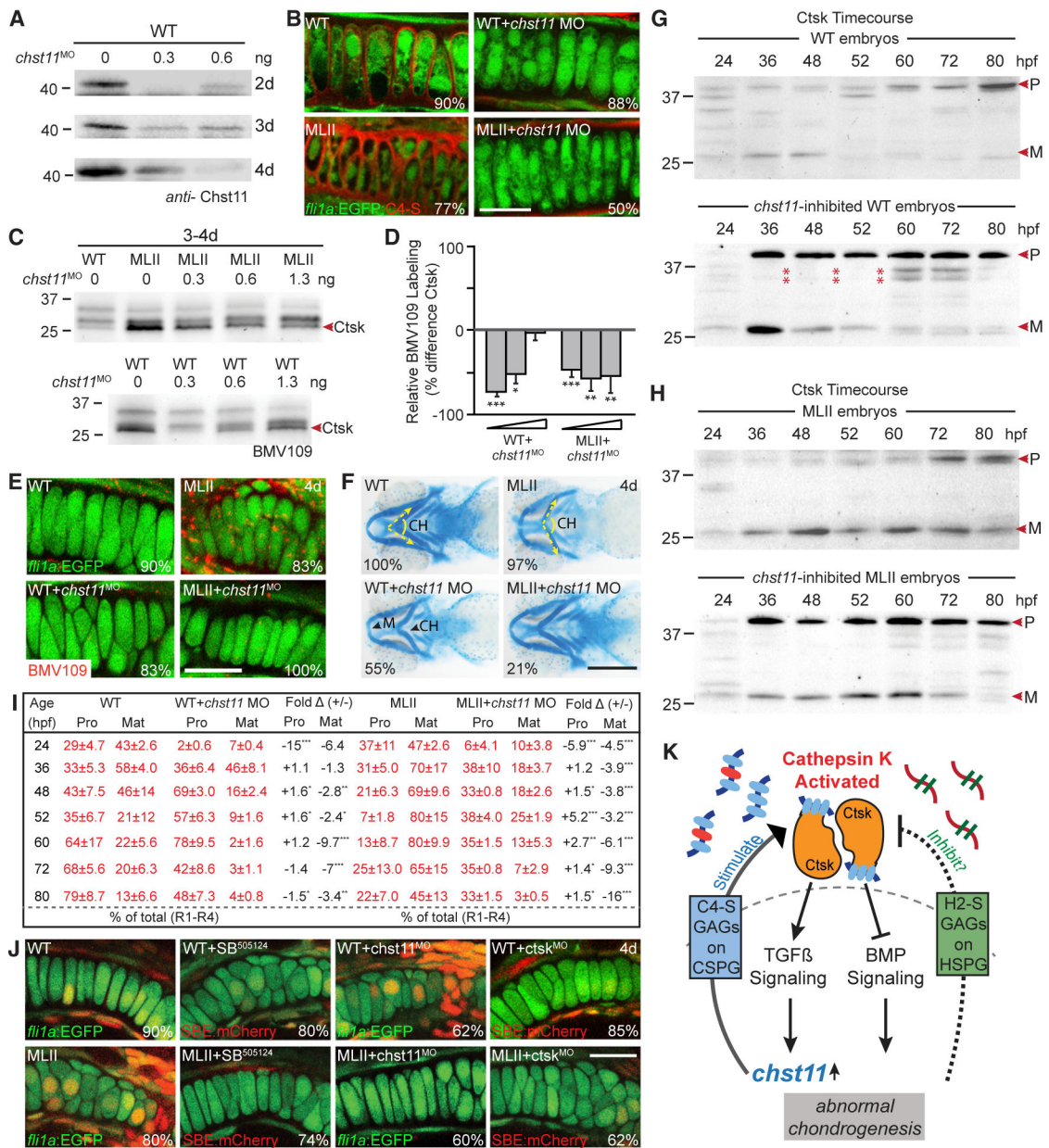
Figure 7. chst11 Inhibition Inhibits Ctsk Processing

(A) Immunoblot of Chst11 in MO-inhibited WT embryos 2–4 d. MLII data and quantitation are shown in Figure S6. n = 3 experiments. d, dpf.

(B) Immunohistochemistry for C4-S (red) in *chst11* MO-inhibited embryos. n = 15–20 embryos per condition from 3 experiments. Percent values are the number of embryos that resemble the picture. Scale bar, 10 μm.

(C) Gels of BMV109-labeled *chst11*-inhibited embryos. n = 4 experiments.

(D) Quantitation of the Ctsk band. Error bars, SD; *p < 0.05, **p < 0.01, ***p < 0.001.

(E) Live confocal analyses of the BMV109 label (red) in *chst11*-inhibited EGFP-positive chondrocytes. n = 10–15 embryos per condition. Percent values are the number of embryos that resemble the picture. Scale bar, 10 μm.

(F) Alcian blue-stained WT, MLII, and *chst11*-inhibited embryos. n = 100–150 embryos per sample from 3 experiments. Percent values are the number of embryos resembling the picture. Scale bar, 10 μm.

(G and H) Immunoblot of Ctsk 24–80 hpf in *chst11*-inhibited WT (G) and MLII (H) embryos. n = 3 experiments.

(I) Table listing the abundance (relative to all Ctsk) of the pro and mature form.

(J) Live confocal analyses of cartilage-localized (green) TGF-β signaling using the SBE:nucCherry reporter. n = 10–15 embryos per condition from 2–3 independent experiments. Percent values are the number of embryos resembling the picture. Scale bar, 10 μm.

(K) Schematic of the current model suggesting that TGF-β-mediated increases in C4-S promote increased activation of extracellular Ctsk in the lysosomal disease MLII. Although not currently known, it is also possible that reduced expression of inhibitory GAGs may contribute. See also Figures S5–S7.